

Article

Developing an Automated Python Surface Energy Balance System (PySEBS) Software for Calculating Actual Evapotranspiration-Software Development and Application Case in Jilin Province, China

Haipeng Liu ^{1,2} , Feng Huang ^{1,2}, Yingxuan Li ^{1,2}, Pinpin Ren ^{1,2}, Gary W. Marek ³, Beibei Ding ^{1,2}, Baoguo Li ^{1,2} and Yong Chen ^{1,2,*}

¹ College of Land Science and Technology, China Agricultural University, Beijing 100193, China

² Key Laboratory of Arable Land Conservation in North China, Ministry of Agriculture and Rural Affairs, Beijing 100193, China

³ USDA-ARS Conservation and Production Research Laboratory, Bushland, TX 79012, USA

* Correspondence: yongchen@cau.edu.cn; Tel.: +86-010-6273-1890; Fax: +86-010-6273-2956

Abstract: In this study, Python Surface Energy Balance System (PySEBS) software was developed in the Python 2.7 programming language for continuous calculation of actual evapotranspiration (ET_a) at regional scales. The software is based on the Surface Energy Balance System (SEBS) model, which uses basic meteorological data, MODIS remote sensing data, and Digital Elevation Model (DEM) data as the original input data and finally outputs daily-scale ET_a in the form of raster data with a spatial resolution of $1\text{ km} \times 1\text{ km}$. To verify the reliability of the PySEBS model, the ET_a of spring maize during the growing season in Jilin Province, China, from 2001 to 2020 was calculated and analyzed in this study and compared with the results of similar studies by others. The findings showed that the PySEBS model has a reasonable accuracy in estimating ET_a within $\pm 15\%$ and is a robust model that can achieve the continuous calculation of ET_a at a regional scale. Therefore, PySEBS software is a useful tool for regional irrigation scheduling and water resources management.

Keywords: PySEBS software; remote sensing data; meteorological data; actual evapotranspiration; spring maize



Citation: Liu, H.; Huang, F.; Li, Y.; Ren, P.; Marek, G.W.; Ding, B.; Li, B.; Chen, Y. Developing an Automated Python Surface Energy Balance System (PySEBS) Software for Calculating Actual Evapotranspiration-Software Development and Application Case in Jilin Province, China. *Remote Sens.* **2022**, *14*, 5629. <https://doi.org/10.3390/rs14215629>

Academic Editors: Yongshuo Fu, Xuan Zhang, Senthilnath Jayavelu, Shengli Tao and Xuesong Zhang

Received: 12 September 2022

Accepted: 4 November 2022

Published: 7 November 2022

Publisher's Note: MDPI stays neutral with regard to jurisdictional claims in published maps and institutional affiliations.



Copyright: © 2022 by the authors. Licensee MDPI, Basel, Switzerland. This article is an open access article distributed under the terms and conditions of the Creative Commons Attribution (CC BY) license (<https://creativecommons.org/licenses/by/4.0/>).

1. Introduction

Actual evapotranspiration (ET_a) is the combined term for ground evaporation and vegetation transpiration. ET_a is an important component of water balance for agricultural fields and is widely used in many areas, such as agronomy, hydrology, ecology, meteorology, and environmental science [1–4]. The influencing factors include meteorological factors such as solar radiation, air temperature, relative humidity, and wind speed. In addition, it is also related to vegetation type, growth condition, and soil properties [5]. The concept closely related to ET_a is the reference crop evapotranspiration (ET_o) [6,7]. The FAO Penman–Monteith approach was developed by defining the ET_o as evapotranspiration from a broad surface of highly uniform, vigorously growing, well-watered green grass, assuming a surface resistance of 70 s m^{-1} , a height of 0.12 m, and an albedo of 0.23 [7].

Since the establishment of Dalton's theorem in 1802, different methods for estimating ET_a have emerged. Bowen et al. [8] proposed the Bowen ratio-energy balance method for ET_a calculation in 1926, according to the energy balance equation. Thornthwaite and Holzman [9] proposed an aerodynamic method for calculating ET_a based on the boundary layer similarity theory. In 1948, Penman proposed the concept of “evaporation force” and established the joint ET_a equation [10]. Monteith [11] derived the famous Penman–Monteith equation in 1965, which opened up a new way to study evaporation from an unsaturated subsurface. Allen et al. [7] used the method of assigning a reference crop

canopy resistance and a fixed height to give a careful description of the use of the P-M formula under different environmental conditions. Subsequently, many studies of stratified models of ET_a were carried out based on the energy balance principle. The single-layer model mainly uses the energy balance residual method, which does not distinguish between soil evaporation and vegetation transpiration in the estimation process. It uses a holistic approach to estimate ET_a , but this method usually results in overestimation under sparse vegetation. Therefore, Shuttleworth and Wallace [12] proposed a two-layer model based on the theoretical principle of the P-M formula, in which soil evaporation and vegetation transpiration are calculated separately. Based on Shuttleworth's two-layer model, Dolman [13] proposed a three-layer model, and Choudhury et al. [14] put forward a four-layer model. Norman et al. [15] developed a two-source model for row crops. All the above methods for calculating ET_a are mainly based on point-source data, which is relatively accurate on small scales. However, in practice, it is often necessary to know the ET_a on a large scale, and the traditional methods can hardly meet the requirements. The gradual rise of remote sensing technology in the late 1960s, especially the application and development of thermal infrared remote sensing, can achieve the conversion from point to surface, which makes the large-scale study of ET_a possible.

A series of remote sensing models for accurate estimation of ET_a have emerged, such as the triangle method model, Surface Energy Balance Algorithm for Land (SEBAL), Surface Energy Balance Systems (SEBS), Mapping Evapotranspiration with Internalized Calibration (METRIC), Two source Trapezoid Model for Evapotranspiration (TTME), Google Earth Engine SEBAL (geeSEBAL), etc. [16–21]. Du et al. [22] used the SEBAL model, combined with remote sensing data and meteorological data, to estimate the water productivity and specific water consumption of rice in the Songnen Plain. Bhattarai and Liu [23] developed a Matlab-based toolbox named LandMOD ET mapper to run SEBAL and METRIC on Landsat and MODIS images for mapping field to regional scale ET_a . The SEBALIGEE model developed by Mhawej and Faour [24] is an automated, user-friendly, flexible, and open-access 30 m ET retrieval system. Its main features are the estimations of ET and K_c in diverse climatic regions with readily available Landsat-8 30-m satellite images. Ramirez-Cuesta et al. [25] developed a new ArcGIS toolbox for implementing the METRIC energy balance model, called Metric-GIS, and tested it in a semi-arid environment. Ellsasser et al. [26] developed the QWaterModel tool based on the DATTUTDUT energy balance model using land surface temperature maps as input, making ET predictions available to a wider audience. Wu et al. [27] introduced an ETWatch Cloud service, which is a model collection migrated from a local PC to the cloud platform for ET generation using readily available RS and standard ground-based meteorological observations. Laipelt et al. [21,28] developed the geeSEBAL software in the Google Earth Engine environment based on the SEBAL algorithm and achieved better results in the calculation of evapotranspiration in the Brazilian region. Huang et al. [29] and Ren et al. [30] used the SEBS model, combined with MODIS data, to estimate the water productivity and water consumption of maize. The results showed that the improved SEBS model could be well applied to the study of ET_a in dryland farming.

Although there are some tools for calculating ET_a at a regional scale, such as ILWIS (Integrated Land and Water Information System) software, the operation process is complicated for users [31]. The purpose of this study is to introduce the Python Surface Energy Balance System (PySEBS) software for calculating ET_a at a regional scale to simplify the complex process of ET_a calculation and to achieve multi-year, continuous, automatic, and efficient estimation of ET_a . Moreover, a case study is performed, and the results of calculated ET_a using this software are described, analyzed, and compared to similar studies.

2. Materials and Methods

2.1. Installing the PySEBS and Software Requirements

The PySEBS is software that can be used to calculate actual evapotranspiration (ET_a) on a spatial scale based on the Surface Energy Balance System model (SEBS). The software is written in Python 2.7.14 due to Python (2.7) being the latest version supported by ArcGIS

10.1–10.6. Since ET_a is calculated on a spatial scale, the software operation utilizes some of the built-in tools in ArcGIS, and the proper operation of these tools depends on the calling of the Arcpy package in ArcGIS. Therefore, the user needs to ensure that the ArcGIS software is installed successfully.

The PySEBS software is compressed into a PySEBS V1.0.0.zip file. The schematic diagram of the PySEBS file structure is shown in Figure 1. The schematic box labeled `./PySEBS/` represents a folder named PySEBS in the working directory, where the PySEBS 1.0.0.zip file will be stored after extraction. The PySEBS folder contains two parts: the PySEBS V1.0.0.exe program; and the site-packages folder containing the code libraries (arcpy package, numpy package, pandas package, Pyshp package, etc.) and the configuration Desktop.pth file.

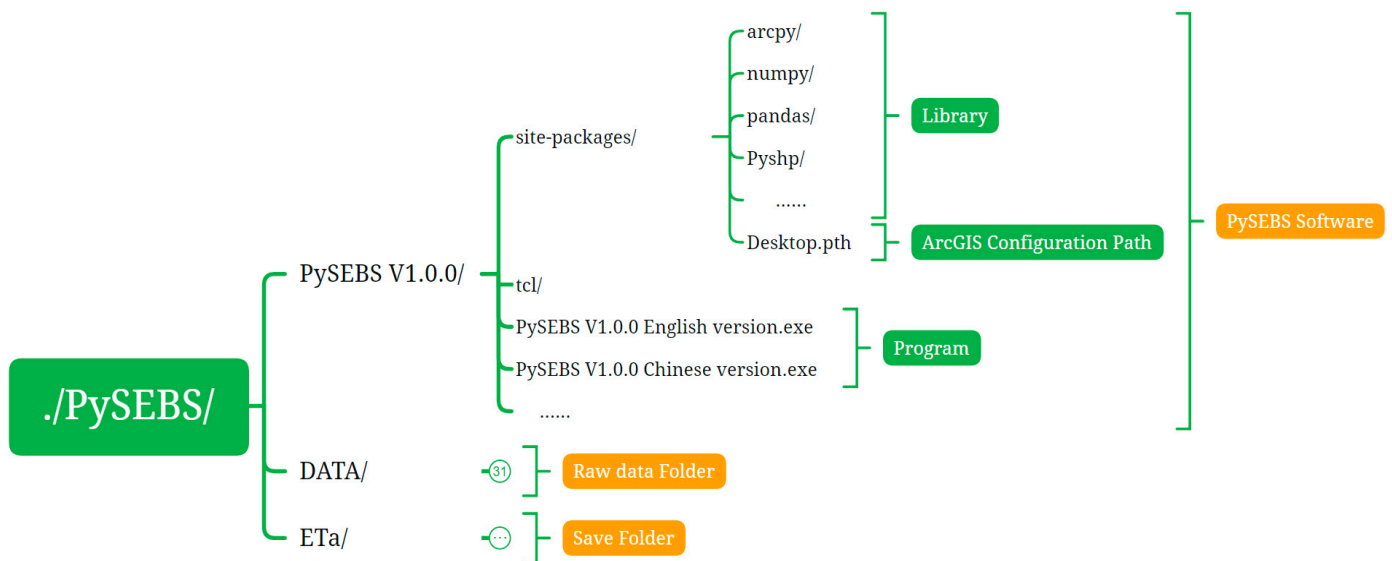


Figure 1. Schematic diagram of the PySEBS software file structure.

2.2. Graphical User Interface Introduction

The PySEBS software is a concise and straightforward scientific computing tool. It contains one main interface and three sub-interfaces (Figure 2). The main interface consists of three button controls: the remote sensing data processing module button, the meteorological data processing module button, and the PySEBS calculation and processing module button. Each button control accesses the corresponding module (sub-interface): Module 1-Remote Sensing Data Processing interface, Module 2-Meteorological Data Processing interface, and Module 3-PySEBS Calculation Procedure interface.

The main functions of Module 1 and Module 2 are to provide properly processed and formatted input data for use in Module 3. Module 3 is used to calculate ET_a on a daily/monthly/annual scale, or for any period of time within a year and across years, based on the input data (raster data) prepared by Modules 1 and 2. There is no processing priority between Modules 1 and 2. Moreover, there are common properties configured for all three modules, including the time setting of the start and end year, file and folder pathway settings, selection of processing method, and information output.

Each module is described below, and detailed descriptions are available in the PySEBS V1.0.0 Actual Evapotranspiration (ET_a) Calculator User's Guide in the Supplementary Materials:

Module 1 is used to process remotely sensed data and generate the daily data files in .asc format for input into Module 3. Module 1 can only process data on an annual basis, and therefore the user must arrange the downloaded remote sensing files in specific folders by data type and by year. The downloaded remote-sensed data needs to be pre-processed before it can be used in the PySEBS program. For demonstration, remotely sensed data were obtained from the National Aeronautics and Space Administration (NASA, <http://modis-land.gsfc.nasa.gov/>

(accessed on 9 March 2019)). In this example, images h26v04 and h27v04 were downloaded, and the MRT (MODIS Reprojection Tool) projection tool was applied to preprocess the data for merging, resampling, format conversion, etc., and Cygwin software was used for batch processing (see Table 1 for specific parameters). The purpose of pre-processing is to convert the remote sensing data from the hierarchical data format (.hdf) to raster files (.tif). The location of the .tif file will be in the same folder as the .hdf file, and the name of the preprocessed .tif file must contain the date information string (seven digits) of the corresponding data; an example file name is MOD09A1_2019001.sur_refl_b01.tif.

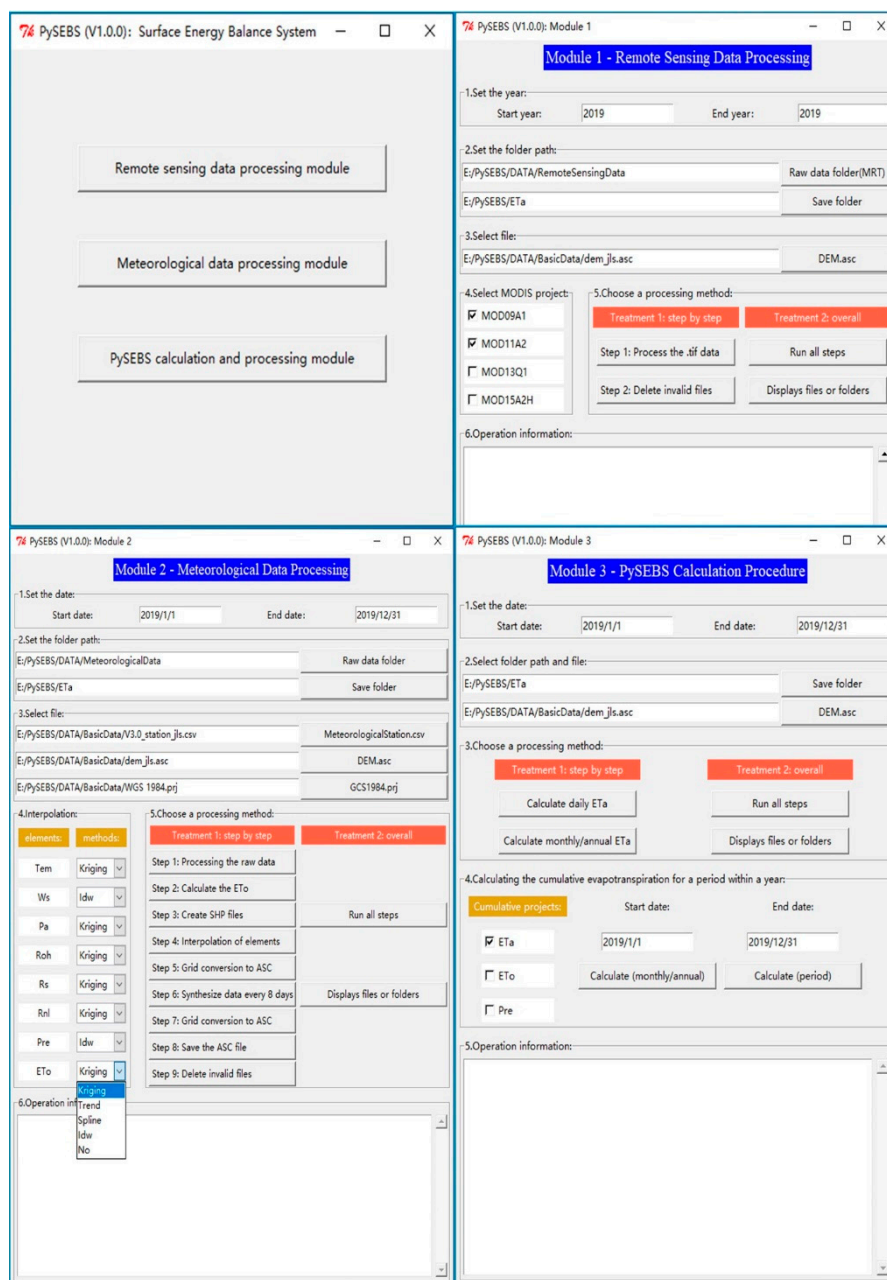


Figure 2. Graphical user interface of PySEBS software. The upper left part is the main menu, the upper right part is the module 1-remote sensing data processing; the lower left part is the module 2-meteorological data processing; and the lower right part is the module 3-PySEBS calculation and processing.

Table 1. Basic information on MODIS products.

Products	Surface Characteristics Parameters	Temporal Resolution	Spatial Resolution
MOD09A1	Surface albedo (Band 1–7) Solar zenith angle (Szen)	8 d	500 m
MOD11A2	Surface temperature (Lst)	8 d	1000 m

The function of Module 2 is to process the meteorological data and generate the daily file in the .asc format that is required by Module 3. The meteorological data used in this study is China's surface climate data daily value data set (V3.0), which is derived from the National Meteorological Information Center (<http://data.cma.cn/site/index.html> (accessed on 30 May 2018)); the platform contains the daily meteorological data from 824 reference weather stations. The meteorological data in the dataset includes atmospheric pressure, air temperature, precipitation, evaporation, sunshine hours, surface temperature, wind speed and direction, and relative humidity at each station. The downloaded original meteorological data is in .txt format and includes all meteorological stations in each folder that need to be preprocessed. Once the downloaded V3.0 weather datasets are placed in the same folder, Module 2 can be used to process the raw data directly. If meteorological datasets from other sources are used, they need to be organized in .csv format and stored in the 1RawData folder. An example of the corresponding path may be: `.\PySEBS\ETa\2MeteorologicalData\1RawData\2019.csv`.

Module 3 uses the daily input data (in .asc format) generated by Module 1 and Module 2 to calculate ET_a on a daily/monthly/annual basis, or for a specified period of time. The PySEBS model requires 15 necessary parameters. Module 1 provides eight essential parameters, including seven parameters from MOD09A1 (Band1, Band2, Band3, Band4, Band5, Band7, and Szen), and one parameter from MOD11A2 (Lst). Module 2 provides seven essential parameters, including the Digital Elevation Model (DEM) parameter and six meteorologically related parameters (Tem, Ws, Pa, Roh, Rs, and Rnl). Moreover, there are two non-essential parameters, Pre and ET_o , which are not involved in the PySEBS calculation process.

2.3. PySEBS Software Theoretical Foundation

The SEBS model, as proposed by Su, is a single-layer model based on the surface energy balance principle [18], which consists of four components: (1) The determination of the land surface physical parameters based on the remotely sensed spectral reflectance and radiance; (2) The estimation of the roughness length for heat transfer; (3) The calculation of sensible heat flux; and (4) The calculation of latent heat flux. Compared with other single-layer models based on the energy balance principle, the PySEBS model has the advantage that the data in each grid is calculated independently, so that even if some grids have missing data on a certain day due to the influence of rain and clouds, the calculation in other grids will not be affected; this can maximize the utilization of the remote sensing data.

The net earth's surface radiation is the basis of various energy exchanges and can be divided into three parts: (1) the soil heat flux that warms the soil; (2) the sensible heat flux that warms the atmosphere; and (3) the latent heat flux of evapotranspiration (the latent heat of soil evaporation and crop transpiration). The main equations for surface energy balance are as follows, and the detailed derivation of the equations can be found in the relevant literature reviewed [7,18,31–42] and in the Supplementary Materials:

$$R_n = G_0 + H + \lambda E, \quad (1)$$

where R_n is the net radiation ($W m^{-2}$), G_0 is the soil heat flux ($W m^{-2}$), H is the sensible heat flux ($W m^{-2}$), and λE is the latent heat flux ($W m^{-2}$), in which λ is the latent heat of evaporation ($J kg^{-3}$) and E is the actual evapotranspiration ($mm d^{-1}$). After calculating each

parameter of the surface energy balance separately, the actual daily ET_a can be obtained according to the constant evaporation ratio within one day.

Calculations of net radiation R_n :

$$R_n = (1 - \alpha) \cdot R_{swd} + \varepsilon \cdot R_{lwd} - \varepsilon \cdot \sigma \cdot T_0^4, \quad (2)$$

where α is surface albedo, a ratio of radiation reflected by the surface to global radiation (a sum of direct solar radiation and scattered radiation); R_{swd} and R_{lwd} ($W m^{-2}$) represent downward solar radiation and downward long-wave radiation, respectively; ε is surface emissivity and can be classified into ε_{land} (surface emissivity of land) and ε_{water} (surface emissivity of water) according to different underlying surfaces; σ is the Stephan Boltzmann constant equal to 5.67×10^{-8} ($W m^{-2} K^{-2}$); and T_0 is the surface temperature (K).

Calculations of soil heat flux G_0 :

$$G_0 = R_n \cdot [\Gamma_c + (1 - f_c) \cdot (\Gamma_s - \Gamma_c)], \quad (3)$$

where Γ_c is the ratio of soil heat flux to net radiation in the condition of total vegetation cover, ($\Gamma_c = 0.05$), and Γ_s is a ratio of soil heat flux to net radiation in the condition of bare soil ($\Gamma_s = 0.315$); f_c is vegetation coverage inversed through remote sensing data.

Calculations of sensible heat flux H :

$$H = \rho C_p \frac{\theta_0 - \theta_a}{r_a}, \quad (4)$$

$$r_a = \frac{1}{ku_*} \left[\ln\left(\frac{z - d_0}{z_{0h}}\right) - \Psi_h\left(\frac{z - d_0}{L}\right) + \Psi_h\left(\frac{z_{0h}}{L}\right) \right], \quad (5)$$

where ρ for air density ($kg m^{-3}$); C_p for constant-pressure specific heat ($J kg^{-1} K^{-1}$); θ_0 for latent surface temperature (K); θ_a for latent air temperature (K) at an elevation of z ; r_a for external resistance; k for Karman constant ($k = 0.4$); u_* for friction velocity ($m s^{-1}$); z for reference measured elevation (m), generally between 2 and 10 m; d_0 for zero plane displacement height (m); z_{0h} for scalar roughness height for heat transfer (m); Ψ_h for stability correction coefficients of heat exchange MOS; and L for Obukhov length (m).

Calculations of daily evapotranspiration E_{daily} :

The previously calculated net surface radiation, soil heat flux, and sensible heat flux are based on the instantaneous values at the moment of satellite transit. In contrast, in the PySEBS model, the daily evapotranspiration is calculated from the evaporation ratio with the daily average net radiation and daily average soil heat flux. The evapotranspiration ratio remains stable throughout the day [43–46], and assuming that the evapotranspiration ratio is constant throughout the day, the daily evapotranspiration is calculated by the following equation:

$$E_{daily} = 8.64 \cdot 10^7 \cdot \frac{24}{0} \cdot \frac{\overline{R_n} - \overline{G_0}}{\lambda \rho_w}, \quad (6)$$

$$\overline{R_n} = (1 - \alpha) K_{24}^\downarrow + \varepsilon L_{24}, \quad (7)$$

$$\overline{G_0} \approx 0, \quad (8)$$

In the above equation, E_{daily} stands for the actual daily evapotranspiration ($mm day^{-1}$); $8.64 \cdot 10^7$ stands for a unit conversion coefficient; $\frac{24}{0}$ stands for the daily mean evaporation ratio that can be substituted by the evaporation ratio Λ figured out by the PySEBS model; $\overline{R_n}$ stands for the daily mean net radiation flux ($W m^{-2}$); and $\overline{G_0}$ stands for the daily mean soil heat flux ($W m^{-2}$), considering that the amount of heat absorbed and released by soil is approximately equal during the day, the daily mean soil heat flux is set to 0. Additionally, λ refers to the latent heat of vaporization of water and $\lambda = 2.45 \cdot 10^6$ ($J kg^{-1}$); ρ_w refers to the density of water and $\rho_w = 1000$ ($kg m^{-3}$); α is the surface albedo; K_{24}^\downarrow refers to

incident global radiation ($W m^{-2}$), which is obtained through the unit conversion of the incident solar radiation ($MJ m^{-2} day^{-1}$) expressed in the Penman–Monteith equation; ε is surface emissivity; and L_{24} refers to daily net outgoing long-wave radiation ($W m^{-2}$), which is obtained through the unit conversion of the net long-wave radiation ($MJ m^{-2} day^{-1}$) expressed in the Penman–Monteith equation.

2.4. Initial Input Data

Input data required by Modules 1, 2, and 3 can be divided into three parts: the first part is the basic data, which includes the information file (V3.0_station_jls.csv) of weather stations for the V3.0 meteorological dataset within the study area, the study area DEM file (dem_jls.asc), and the geographic coordinate system file (WGS 1984.prj); the second part is the remote sensing data, which includes MOD09A1 and MOD11A2; the third part is the meteorological data, which includes the raw data of the V3.0 meteorological dataset. Meteorological data from other sources can also be used; the data needs to be prepared by the users following the format of 2019.csv and located in the corresponding folder.

The input data or files described above are all saved in the designated folders. Each module is connected to the file or folder so that the data can serve as the input for the module. Specifically, the basic data is connected in the form of files; remotely sensed data and meteorological data are connected in the form of subdirectory.

The structure diagram of the path to the initial input data is shown in Figure 3. The path to the basic data is `./PySEBS/DATA/BasicData/`. The path to the remote sensing data is `./PySEBS/DATA/RemoteSensingData/MOD09A1/2019/` and `./PySEBS/DATA/RemoteSensingData/MOD11A2/2019/`. The meteorological data is saved in the path: `./PySEBS/DATA/MeteorologicalData/`.

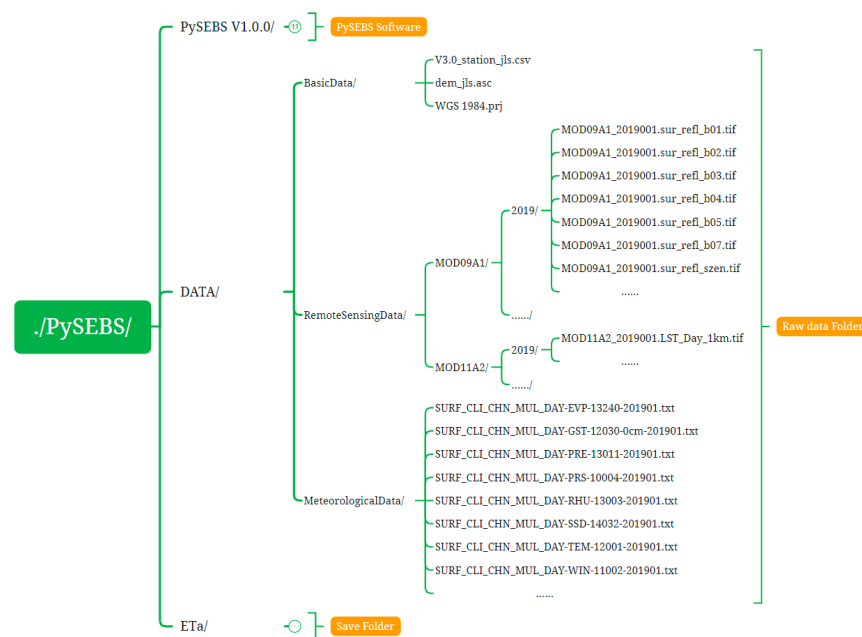


Figure 3. Structure of the path to the initial input data.

2.5. Output Results

The `./PySEBS/ETA/` file path is a user-defined folder to save the output results, which will be created automatically if such a folder does not exist in the project directory. The folder `1RemoteSensingData/` is used to save the intermediate files generated during the remote sensing data processing in Module 1. The folder `2MeteorologicalData/` is used to save the intermediate files generated during the meteorological data processing in Module 2. The folder `3PySEBSInputData/` is used to save the final processing results of remote sensing and meteorological data. In addition, the folder `3PySEBSInputData/` also serves as the

path for input files for Module 3. The 4PySEBSOutputData/ folder will store the daily ET_a results, and the 5sum_ ET_a / folder will store the monthly and annual ET_a results calculated by Module 3 (Figure 4). The 6sum_ ET_o / folder and the 7sum_Pre/ folder are used to store cumulative reference evapotranspiration and precipitation, respectively.

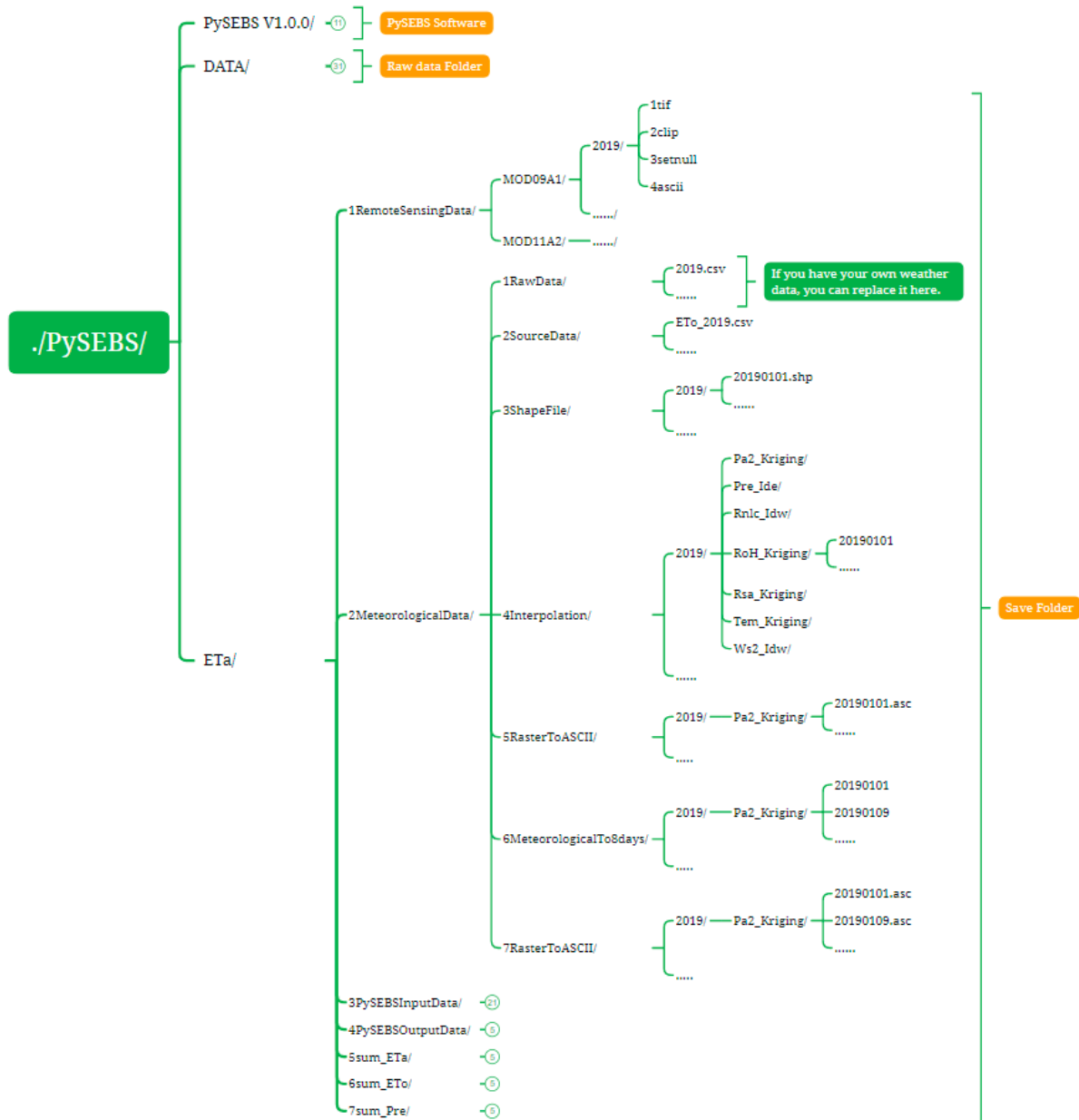


Figure 4. Schematic diagram of the structure of folder 1RemoteSensingData/ and folder 2MeteorologicalData/.

As mentioned earlier, if meteorological data derived from other sources need to be used, the data must be prepared in the required format (Figure 5) and stored in the file path 2Meteorologicaldata/1RawData/ to replace the V3.0 meteorological data. The files in the file path 2MeteorologicalData/2SourceData/ (e.g., ETo_2019.csv) used the data in the 2Meteorologicaldata/1RawData/ folder as input and calculated the ET_o and its process variables; the purpose of these files is to provide the six required meteorological parameters for Module 3. The calculation of ET_o is also a strength of this software, if the users need to use ET_o and other parameters in the calculation process, the information can be found in the folder 2MeteorologicalData/2SourceData/.

	A	B	C	D	E	F	G	H	I	J	K	L	M	N	O	P	Q	R
1	no	pro	city	lat	lon	alt	year	month	day	Tmax	Tmin	Tem	Ws	Pa	Rh	Sh	Pre	R
2	50877	HJ	YL	46.3	129.58	100.1	2019	1	1	-11.8	-17.9	-15.1	5.98	101.58	50	0.9	0	
3	50877	HJ	YL	46.3	129.58	100.1	2019	1	2	-9.8	-18.8	-14.3	3.07	101.7	62	7	0	
4	50877	HJ	YL	46.3	129.58	100.1	2019	1	3	-8	-15.6	-12.5	3.81	101.85	60	7.1	0	
5	50877	HJ	YL	46.3	129.58	100.1	2019	1	4	-7.4	-16.2	-11.7	3.44	101.04	70	4.8	0.4	
6	50877	HJ	YL	46.3	129.58	100.1	2019	1	5	-11.1	-16.1	-14.2	3.74	101.27	60	7	0	
7	50877	HJ	YL	46.3	129.58	100.1	2019	1	6	-10.3	-18.5	-14.8	3.44	101.64	58	7.1	0	
8	50877	HJ	YL	46.3	129.58	100.1	2019	1	7	-10.6	-19.6	-15.1	2.17	101.21	56	4.9	0	
9	50877	HJ	YL	46.3	129.58	100.1	2019	1	8	-10.7	-19.3	-14.9	3.81	101.14	57	6.7	0	
10	50877	HJ	YL	46.3	129.58	100.1	2019	1	9	-6.2	-16.1	-11.1	4.86	100.68	45	7.1	0	
11	50877	HJ	YL	46.3	129.58	100.1	2019	1	10	-3.3	-14.3	-8.9	3.22	100.54	53	7.3	0	
12	50877	HJ	YL	46.3	129.58	100.1	2019	1	11	-4.3	-19.6	-12.9	1.35	101.3	64	7.3	0	
13	50877	HJ	YL	46.3	129.58	100.1	2019	1	12	-3.4	-20.3	-14.3	0.45	101.16	67	7.1	0	
14	50877	HJ	YL	46.3	129.58	100.1	2019	1	13	-10.9	-19.1	-14.9	0.9	101.31	74	0	0	
15	50877	HJ	YL	46.3	129.58	100.1	2019	1	14	-7.7	-16.7	-11.5	1.27	101.14	75	0	0	
16	50877	HJ	YL	46.3	129.58	100.1	2019	1	15	-8.5	-17.5	-12.2	2.77	100.78	62	3.8	1.9	
17	50877	HJ	YL	46.3	129.58	100.1	2019	1	16	-10.6	-18.1	-15	4.11	100.3	51	4.6	0	
18	50877	HJ	YL	46.3	129.58	100.1	2019	1	17	-15.7	-23.6	-20.3	4.86	100.88	39	7.8	0	
19	50877	HJ	YL	46.3	129.58	100.1	2019	1	18	-12.2	-21.5	-17.3	3.22	101.38	45	7.9	0	
20	50877	HJ	YL	46.3	129.58	100.1	2019	1	19	-7.1	-23.8	-15.7	1.94	100.81	52	7.4	0	
21	50877	HJ	YL	46.3	129.58	100.1	2019	1	20	-11.3	-18.2	-15	2.77	100.33	62	3.1	0	
22	50877	HJ	YL	46.3	129.58	100.1	2019	1	21	-8.3	-22.7	-15.3	1.2	100.16	59	8	0	
23	50877	HJ	YL	46.3	129.58	100.1	2019	1	22	-4	-17.4	-9	2.77	99.8	56	0.9	0	
24	50877	HJ	YL	46.3	129.58	100.1	2019	1	23	-6.7	-13.8	-11.3	3.37	100.44	58	3.7	0	
25	50877	HJ	YL	46.3	129.58	100.1	2019	1	24	-7.5	-18.7	-12.7	2.54	101.19	55	7.9	0	
26	50877	HJ	YL	46.3	129.58	100.1	2019	1	25	-7	-15.2	-11.7	1.57	101.3	64	7.2	0	
27	50877	HJ	YL	46.3	129.58	100.1	2019	1	26	-6.1	-16.6	-11.6	2.54	101.32	62	8.2	0	
28	50877	HJ	YL	46.3	129.58	100.1	2019	1	27	-1.3	-10.4	-6.9	4.11	100.24	46	6.1	0	
29	50877	HJ	YL	46.3	129.58	100.1	2019	1	28	-6.8	-14	-10.6	4.11	100.22	61	7	0	
30	50877	HJ	YL	46.3	129.58	100.1	2019	1	29	-3.1	-16.8	-11.2	1.27	100.93	61	5	0	

Figure 5. The example format of the meteorological data in replacement for the V3.0 data in 1RawData/.

The 3PySEBSInputData/ folder stores the final processing results calculated from Module 1 and Module 2 and the input files from Module 3. The files are stored in the form of one folder per day and contain 15 .asc files that are required for the PySEBS model calculation and one optional precipitation file (pre.asc). The required parameters include one DEM file (dem.asc), seven MOD09A1 files (band1.asc, band2.asc, band3.asc, band4.asc, band5.asc, band7.asc, and szen.asc), one MOD11A2 file (lst.asc), and six meteorological parameter files (tem.asc, ws.asc, pa.asc, roh.asc, rs.asc, and rnl.asc) (Figure 6).

2.6. PySEBS Case Study-Study Area

After the development of PySEBS software, the ET_a was calculated for spring maize in Jilin Province from 2001 to 2020, and the ET_a was analyzed at both temporal and spatial scales during the growing season of spring maize in this study. Jilin Province is located in the central part of northeastern China (Figure 7). The terrain map shows obvious characteristics of high elevations in the southeast and low elevations in the northwest. The latitude varies from $40^{\circ}50'$ to $46^{\circ}19'N$, and the longitude ranges from $121^{\circ}38'$ to $131^{\circ}19'E$. Jilin Province is 769.6 km long from east to west and 606.6 km wide from north to south and has an area of 187,400 km². As for climate conditions, it belongs to a temperate continental monsoon climate with four distinct seasons. Rain and heat are in the same season, such as a rainy summer with high temperatures and a cold and dry winter. The average winter temperature is below $-11^{\circ}C$, and the average summer temperature is above $23^{\circ}C$. The annual average sunshine hours are 2259–3016 h. The annual average precipitation is 400–600 mm, and the annual frost-free period is 120–160 days. The climatic conditions of Jilin Province make it an important commodity grain production region in China. Due to the geographical advantage for agriculture, it has become one of the three famous Corn Belts in the world.

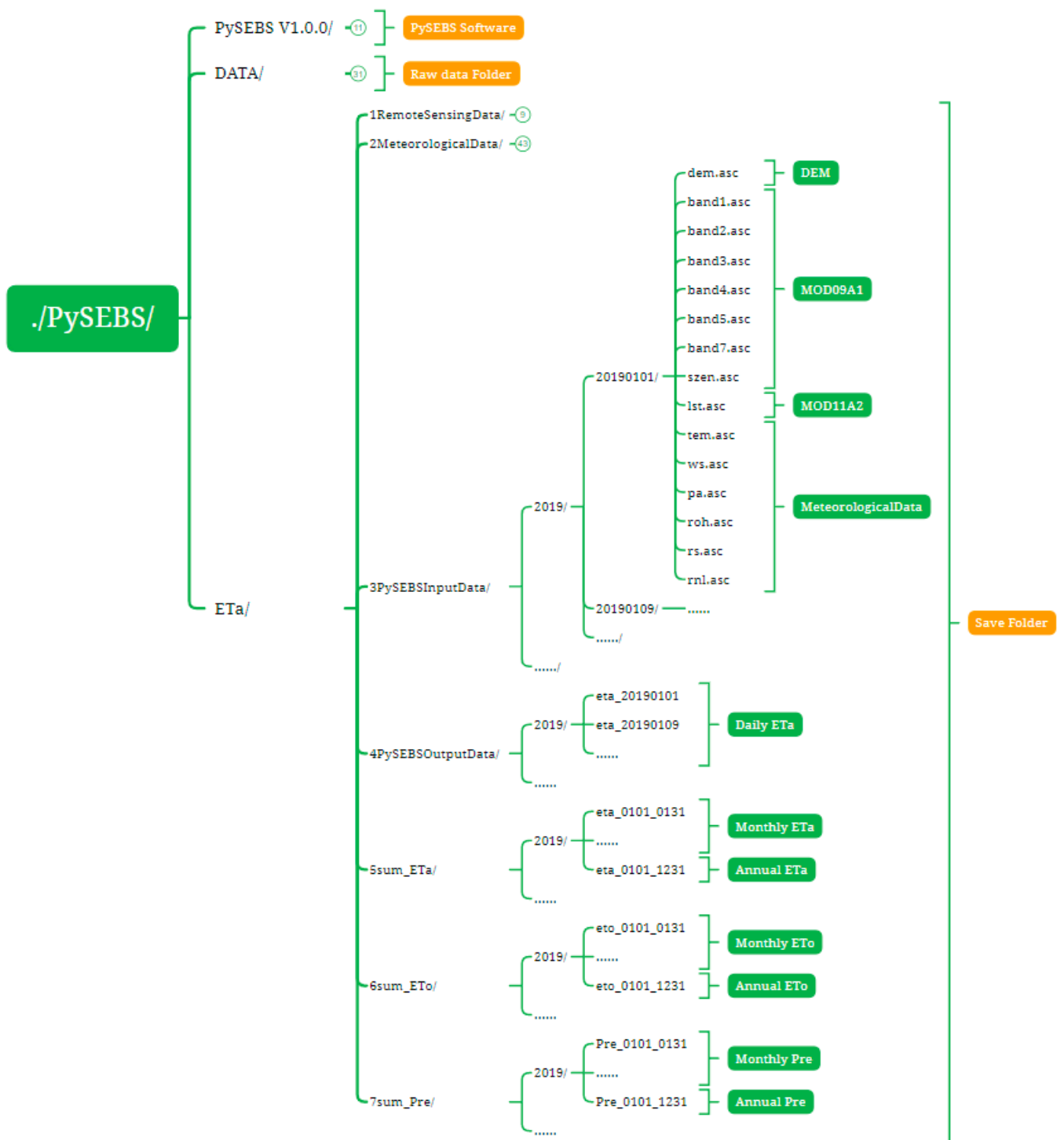


Figure 6. Schematic diagram of the structure of folders 3PySEBSInputData/, 4PySEBSOutputData/, and 5sum_ETa/, 6sum_ETo/, and 7sum_Pre/.

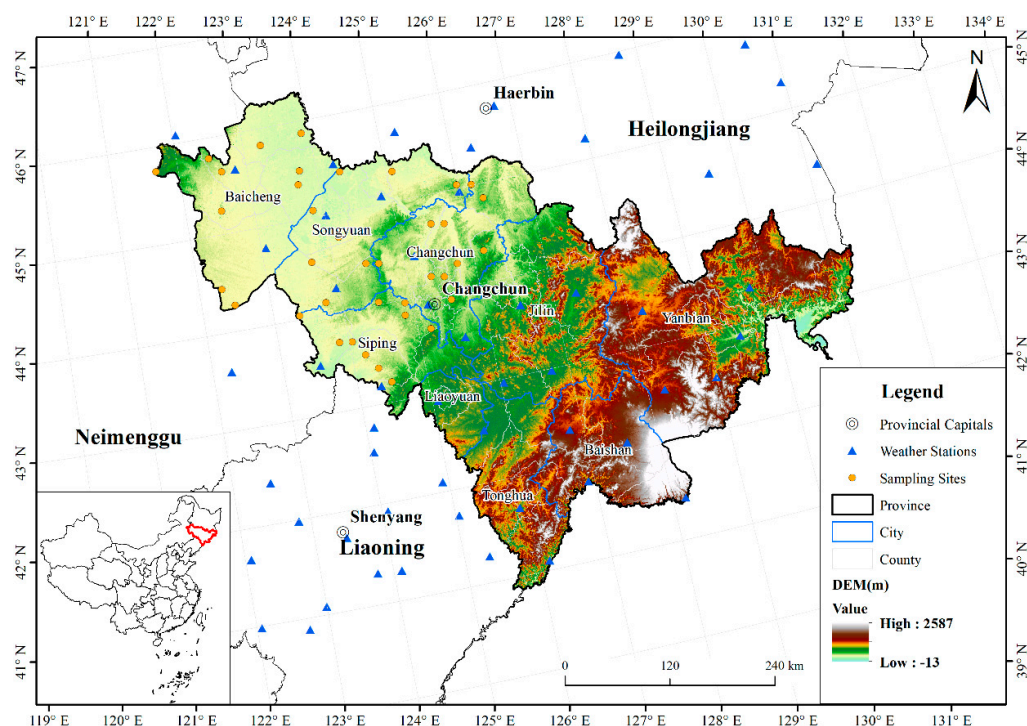


Figure 7. Location of the study area, sampling sites for extraction of planting area, and DEM map.

2.7. Calculation of ET_a during Spring Maize Growing Season

The ET_a of spring maize was calculated by PySEBS software. The data used were remote sensing data, meteorological data, and DEM data. The remote sensing data were obtained from NASA. The meteorological data are the daily data set of China's surface climate data (V3.0), which were accessed from the Chinese National Meteorological Information Center. The digital elevation data ASTER GDEM V2 were downloaded from the geospatial data cloud (<http://www.gscloud.cn/> (accessed on 16 May 2018)) with a spatial resolution of $30\text{ m} \times 30\text{ m}$.

In the process of calculating ET_a through the PySEBS model in this study, the weather data were synthesized for 8 days due to the remote sensing data of MOD09A1 and MOD11A2 used are 8-day synthesis products. Then, the weather data and remote sensing data with a unified time scale were used as the input parameters of the PySEBS model. Finally, the 8-day synthetic ET_a was obtained. Then, according to the start and end time of the growth period of spring maize (1 May to 30 September), the ET_a during the growth period was accumulated by adding up.

3. Results

3.1. Extraction of Planting Area

The PySEBS software is a software for the calculation of the ET_a on a spatial scale, and the results of the calculation are finally presented in the form of a raster dataset. Since the subject of research in this study is spring maize in Jilin Province, the planting area of spring maize in the study area needs to be determined first.

According to the distinct spectral characteristics of spring maize in different growth stages, the Normalized Difference Vegetation Index (NDVI) can effectively reflect the differences between various crops. Based on the curve of the MODIS-NDVI time series and the land use data of Jilin Province over 16 years, a decision tree classification model was constructed to achieve the extraction of the spring maize planting area. To obtain time series curves of NDVI of spring maize in Jilin Province for all years, the NDVI values of each sampling site were extracted as the main basis for extracting the spring maize planting

area using the coordinate information of 38 sample sites with a long-term spring maize planting in this study (Figure 7).

After the sowing and emergence stages, the NDVI showed an increasing trend, which rose rapidly during the three-leaf, seven-leaf, and jointing stages of the spring maize vegetative growing period. When the spring maize entered the tasseling stage at the peak of vegetative growth, the NDVI value reached its peak. Then, spring maize entered the reproductive growth stages of the silking period, milk maturity period, and maturity period, during which the NDVI values gradually decreased. To eliminate the influence of noise on the NDVI values, the method of Harmonic Analysis of Time Series (HANTS) was used to smooth the time series of MODIS-NDVI. The comparison of before and after processing curves is shown in Figure 8.

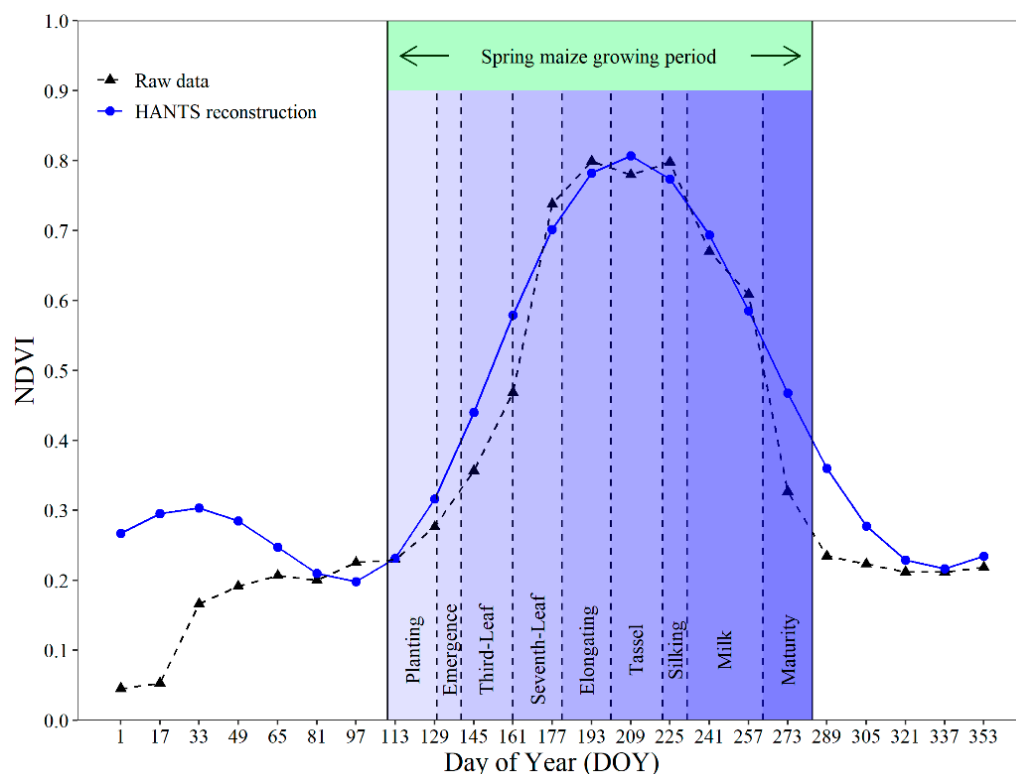


Figure 8. Comparison of before and after MODIS-NDVI time series reconstruction of spring maize.

The construction of the decision tree for the extraction of the spring maize planting area in Jilin Province was based on the minimum and maximum time series curves of NDVI for the period of 2001 to 2016. A total of 13 images of NDVI values reconstructed by HANTS using a day-of-year (DOY) calendar from DOY 113 to 305 over 16 years were selected for this study. The pixels between the minimum and maximum NDVI values of the corresponding DOY were the candidate areas for the spring maize planting area. To eliminate the influence of other land uses, the agricultural land in the land cover map provided by the remote sensing data of MCD12Q1 was extracted as a mask. Finally, the spring maize planting area was obtained. The extraction process is shown in Figure 9.

In this study, the identification of the spring maize planting area was based on the NDVI time series curve for the period of 2001 to 2016. Except for 2003 and 2014, the extraction area and statistical area of 56 counties and districts in Jilin Province were basically evenly distributed on both sides of the 1:1 line, indicating that the constructed decision tree could better extract the planting area of spring maize (Figure 10). The relative error of spring maize area extraction from 2001 to 2016 was -4.15% . The lowest extraction accuracy over the years was above 80%, and the average extraction accuracy reached 90.60%. The coefficient of determination (R^2) values of the statistical area and the extracted area of

spring maize were greater than 0.8 except for 2001 to 2003, and the overall R^2 was 0.81, which indicated that the extraction method of the spring maize area used in this study fit well with the actual situation.

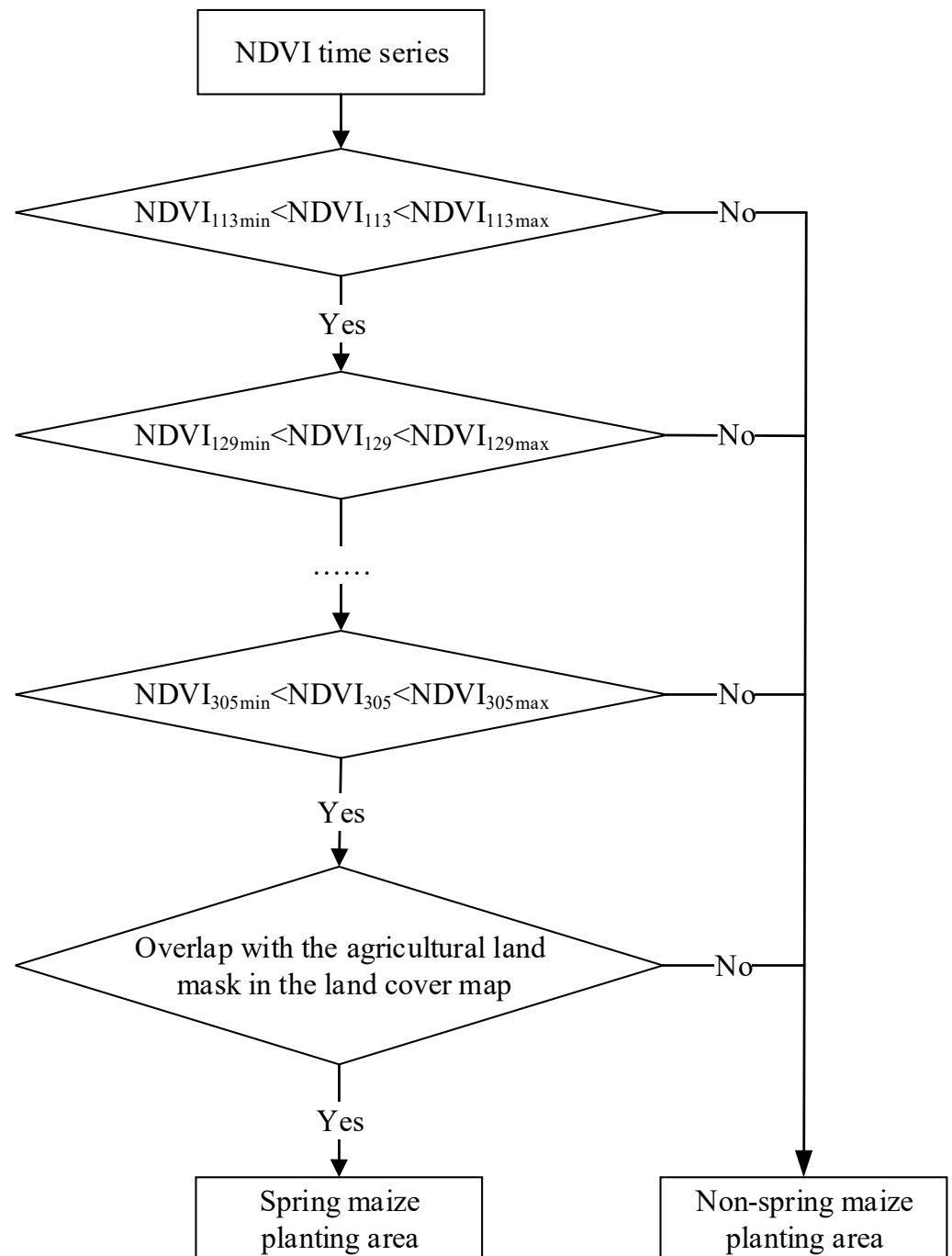


Figure 9. Schematic map of decision tree classification extraction for spring maize planting area.

The map of the multi-year average spring maize planting area in Jilin Province was obtained by accumulating the raster files of planting areas in previous years, and a raster was considered to belong to the multi-year average spring maize planting area when the number of years in which a raster appeared exceeded 7 years. This planting area map was used to clip the ET_a raster data of Jilin Province calculated by PySEBS software to obtain the ET_a of spring maize.

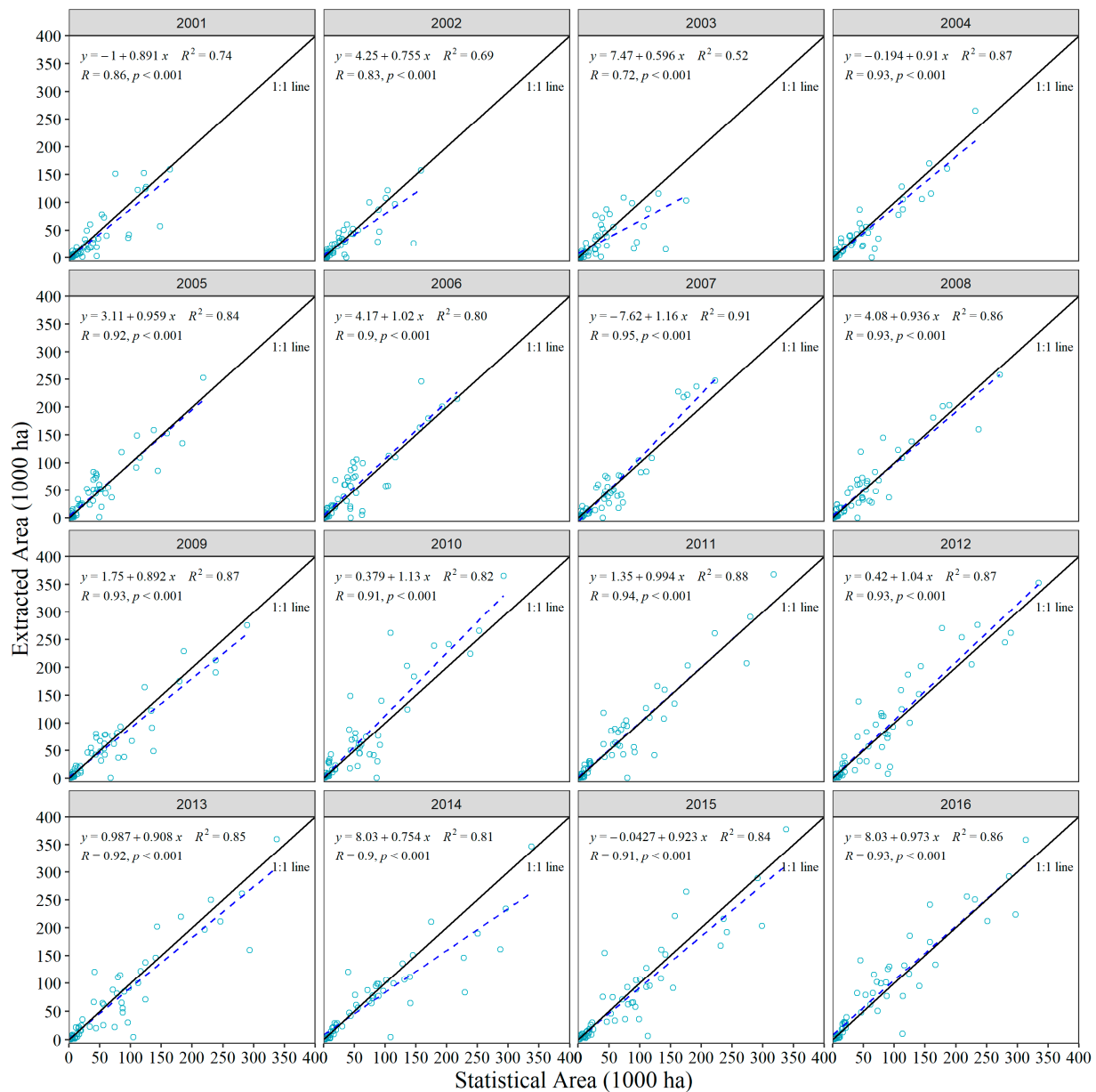


Figure 10. Results of planting area extraction for spring maize.

3.2. Temporal and Spatial Distribution Patterns of ET_a

The temporal distribution pattern of ET_a during the spring maize growing period (May to September) from 2001 to 2020 in Jilin Province is shown in Figure 11. The average cumulative ET_a during the growing period of spring maize in Jilin Province ranged from 475 to 544 mm, with a multi-year average value of 517 mm and an average standard deviation value of 43 mm (Figure 11A). The lowest and highest ET_a happened in 2008 and 2020, respectively. The average annual cumulative ET_a differed from 632 to 694 mm, with a mean value of 666 mm, and the standard deviation varied from 50 to 86 mm, with a mean value of 65 mm (Figure 11B). The monthly distribution pattern of ET_a showed a trend of increasing and then decreasing, with the monthly average ET_a of 2, 9, 34, 58, 83, 110, 132, 114, 78, 35, 9, and 2 mm from January to December, respectively, with the highest value of ET_a in July. The cumulative ET_a was 517 mm from May to September during the spring maize growing period (Figure 11C).

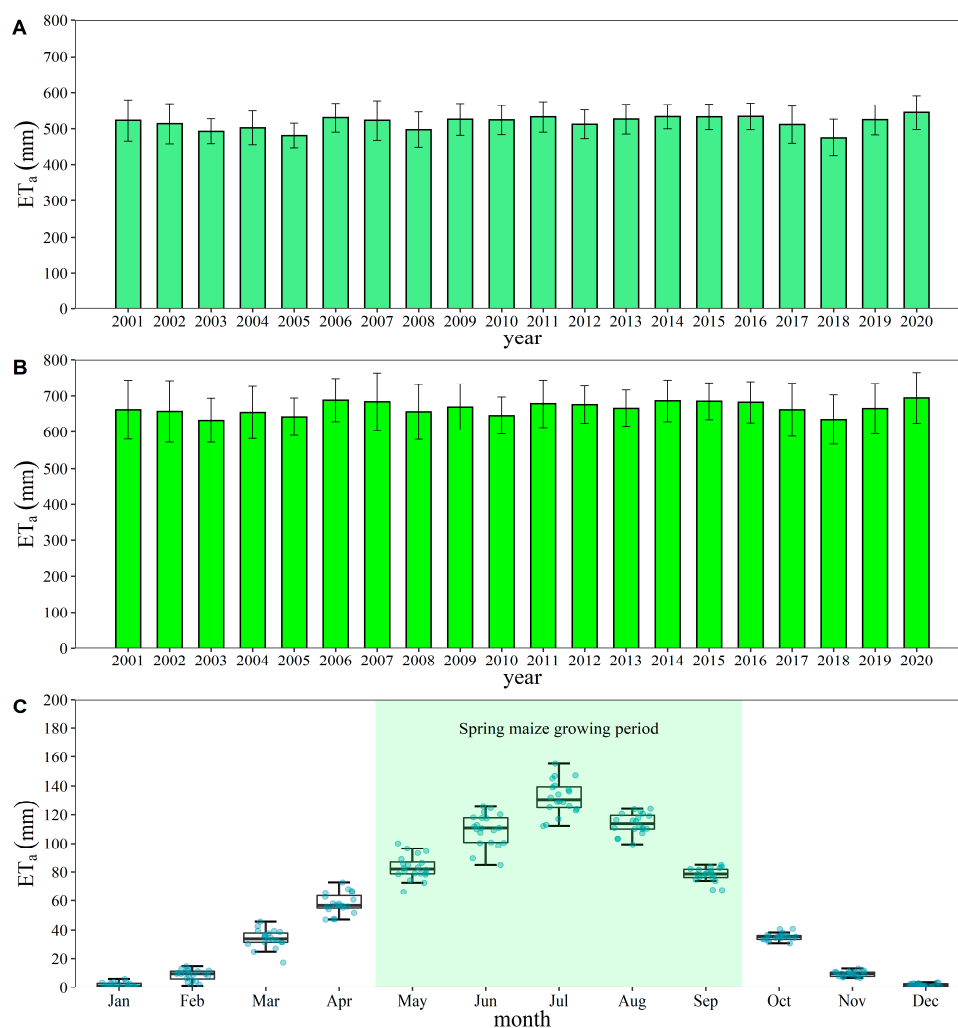


Figure 11. Temporal distribution pattern of ET_a of spring maize in Jilin Province from 2001 to 2020. (A) Cumulative ET_a during the spring maize growing periods for all years (1 May to 30 September); (B) cumulative ET_a throughout the year in the spring maize growing area for all years (1 January to 31 December); (C) monthly distribution of ET_a over the spring maize growing area for 20 years, where the shaded part represents the spring maize growing period. Data are presented as mean plus or minus standard deviation.

The spatial distribution of the multi-year average ET_a and inter-annual coefficient of variation (CV) of spring maize in Jilin Province from 2001 to 2020 is shown in Figure 12. The multi-year average ET_a was between 391 and 693 mm in Jilin Province, and the multi-year average ET_a in Changchun City, Siping City, Jilin City, Liaoyuan City, and other regions was between 450 and 550 mm. Farmland near rivers, such as the Dongliao River in Siping City, the Songhua River across Songyuan City and Changchun City, and the Nen River across the border of Baicheng City, had the ET_a above 600 mm. Areas with annual average ET_a less than 450 mm were mainly distributed in the western region of Jilin Province, such as Baicheng City, Songyuan City, and the eastern part of Siping City. This might be because these areas had mostly sandy soil and insufficient rainfall. The CV of the multi-year average ET_a of spring maize was mostly between 2% and 18% in Jilin Province. In a few areas, such as the western part of Baicheng City and Songyuan City, the inter-annual CV exceeded 10%, which might be caused by the large variation in inter-annual rainfall in these areas. Figure 13 shows the distribution of ET_a during the growing season of spring maize in Jilin Province in all years: the ET_a was lower in 2005, 2008, and 2018 compared to other years,

and the ET_a in the rest of the years was relatively stable and maintained between 450 and 550 mm.

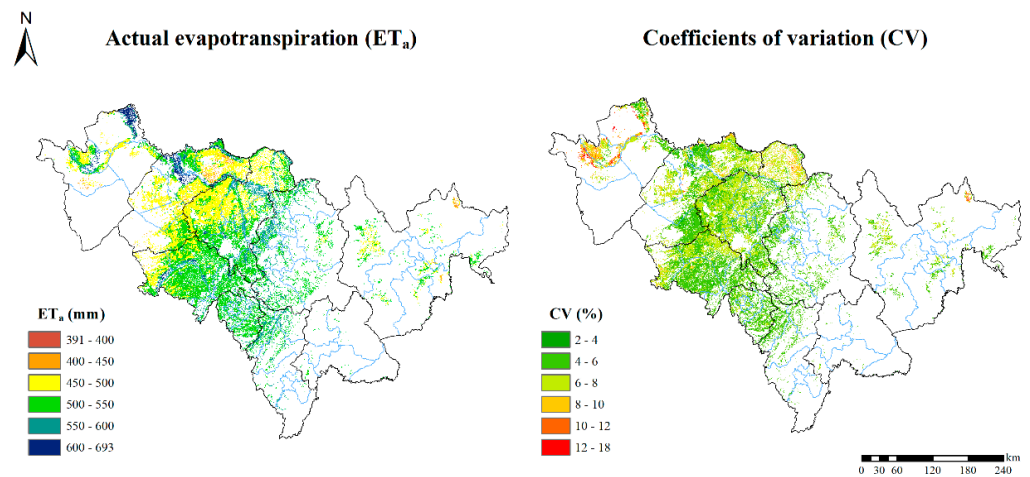


Figure 12. Multi-year average ET_a (2001–2020) and its coefficient of variation (CV) during the growing period of spring maize in Jilin Province.

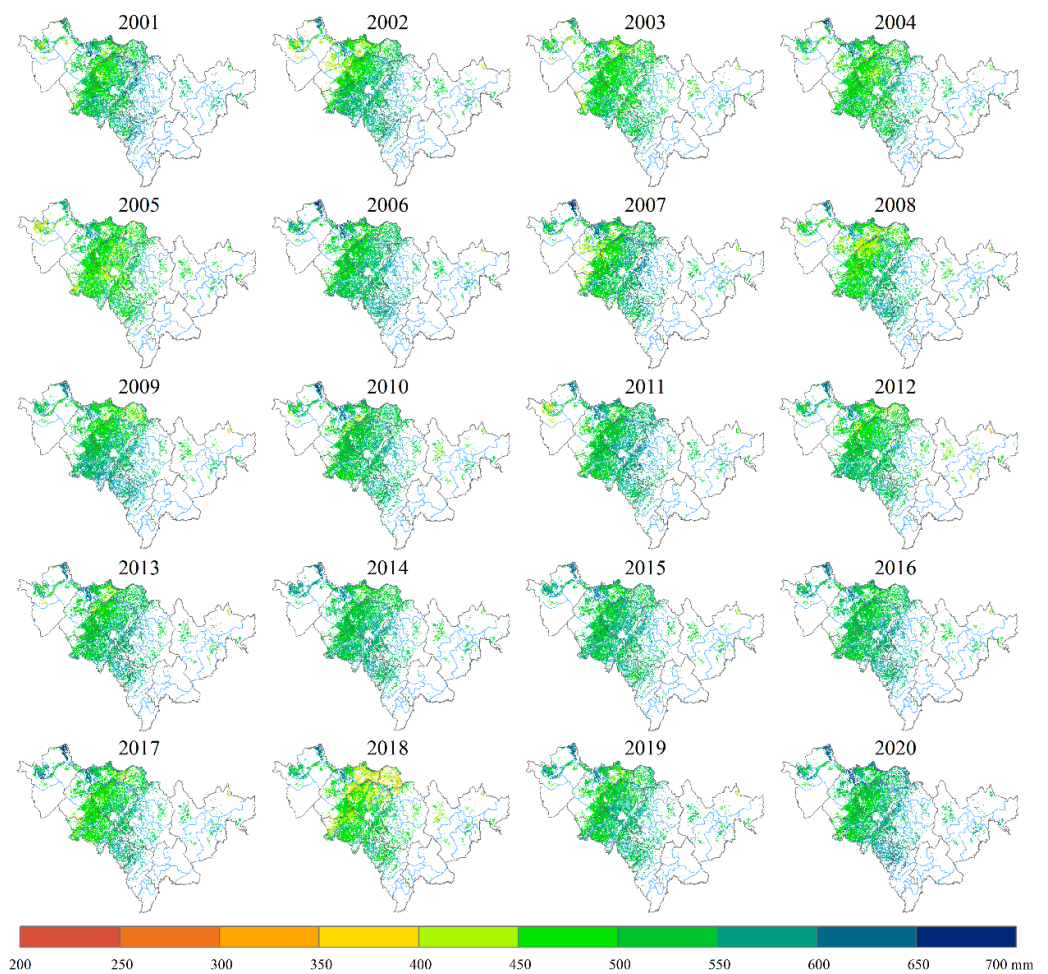


Figure 13. ET_a of spring maize during growing season over the years.

The ET_a values for each city in Jilin Province are shown in Figure 14. ET_a for the spring maize growing season in each city basically remained between 450–550 mm from 2001 to 2020, and the largest multi-year average ET_a was in Tonghua, Jilin, and Liaoyuan with ET_a

exceeded 530 mm. The smallest ET_a was in Yanbian, Songyuan, and Changchun with an ET_a lower than 510 mm (Figure 14A). The CV of ET_a for the spring maize growing season in each city ranged from 5% to 8%, with the smallest variability being 5% in Tonghua and the largest variability being 7.8% in Baicheng (Figure 14B). The distribution of ET_a by month in each city is shown in Figure 14C. ET_a was mainly concentrated in May–September, i.e., during the growing period of spring maize, and reached its maximum in July with an average of approximately 150 mm.

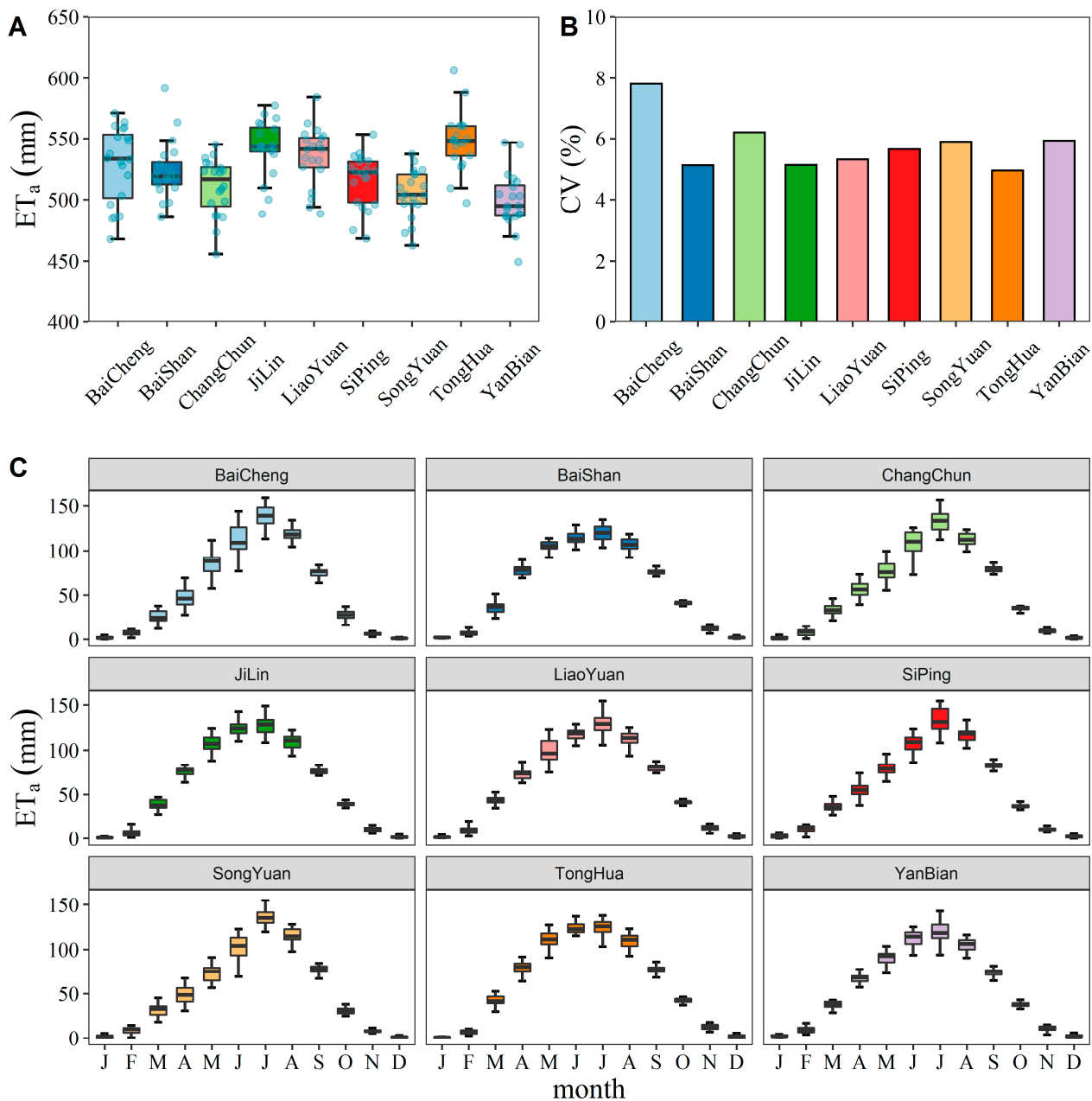


Figure 14. ET_a of spring maize in each city of Jilin Province. (A) Multi-year average ET_a in each city during the spring maize growing season from 2001 to 2020, (B) coefficient of variation (CV) of ET_a during the spring maize growing season in each city from 2001 to 2020, and (C) monthly ET_a in each city.

4. Discussion

4.1. Comparison of the Calculated ET_a Results with Similar Studies

To verify the rationality of the ET_a calculation results, this study has gathered and sorted out related studies for comparison (Table 2). Guo et al. [47] estimated the ET_a of spring maize in Yushu City, Jilin Province, in 2013, using a large weighing lysimeter on a farm scale, and found an average value of 362 mm for ET_a . Qiu et al. [48] and Zhang et al. [49] used the Penman–Monteith and crop coefficient method to estimate the 3-year and 54-year ET_a of spring maize in Jilin Province, and the average values were 523 mm and 538 mm, respectively, which were similar to the results of this study. Liu [50] used the SIMETAW (Simulation Evapotranspiration of Applied Water) model to simulate the evapotranspiration of the spring maize growing season under different hydrological year types in western Liaoning from 2007 to 2009, and the results were 464 mm, 485 mm, and 486 mm in abundant, flat, and dry years, respectively.

Table 2. Comparison of the PySEBS estimated spring maize ET_a with similar studies (unit: mm).

Study Method	Scale	Crop	Value Range	Mean	Period	Area	Source
Weighting lysimeter	Farmland	Spring maize	-	362	2013	Yushu City, Jilin Province	Guo, [47]
Penman–Monteith + Crop coefficient method	Regional	Spring maize	452–637	523	1981–2014	Jilin Province	Qiu, [48]
Penman–Monteith + Crop coefficient method	Regional	Spring maize	455–641	538	1961–2015	Midwest Jilin Province	Zhang, [49]
SIMETAW Model	Regional	Spring maize	464–486	480	2007–2009	Fuxin, Liaoning Province	Liu, [50]
PySEBS Model	Regional	Spring maize	391–693	517	2000–2017	Jilin Province	This study

In this study, the ET_a values of spring maize in Jilin Province from 2001 to 2020 were between 391 mm and 693 mm, with a multi-year average of 517 mm. This was similar to the results of other related studies in Jilin Province. Jiang et al. [51] pointed out that the maximum error value of ET_a estimated by using remote sensing data is reasonable within $\pm 20\%$. However, Seguin et al. [52] suggested that the maximum error of ET_a estimated by remote sensing changes with the actual applications, and the absolute value is usually reasonable around 15–30%. Since there is no relevant flux tower data in the study area that can be used directly for the validation of this model for ET_a estimations, a relevant literature review was conducted to validate the estimation effectiveness of this PySEBS model on ET_a in Jilin Province. The results of relevant literature studies on spring maize ET_a in Jilin Province at the regional scale were 514 mm on average, while the average result of the PySEBS model was 517 mm, with a relative error of less than 1%, indicating a good applicability of the modified model in regional studies (Table 2).

PySEBS software has a high application value in water use evaluation and irrigation management. Based on this model, Ren et al. [30] studied the spatio-temporal patterns of water consumption and irrigation demand during winter wheat-summer maize agricultural production in the Huang-Huai-Hai Plain (3HP), and the scenario analysis of different cropping methods was evaluated. The annual average ET_a of winter wheat-summer maize ranged from 700–900 mm with no significant change, while irrigation water demand showed a large interannual variation. In addition, four alternatives that may require less irrigation were tested, i.e., wheat-maize-wheat-fallow (WMWF), wheat-maize-fallow-maize (WMFM), wheat-maize-fallow-spring maize (WMFSM), and fallow-spring maize-fallow-spring maize (FSMFSM), with the results showing that FSMFSM has the best water savings, reducing irrigation by 64%.

4.2. Advantages and Disadvantages of PySEBS Software

Before the development of PySEBS software, studies were conducted by calculating regional ET_a using the SEBS module embedded in ILWIS software (<https://52north.org/software/software-projects/ilwis> (accessed on 1 April 2019)), but the SEBS module has many shortcomings, such as a tedious calculation process, inefficient calculation, only one period of results can be calculated at one time, a lack of batch processing capability, and various coefficient transformations of data are required during processing to make the data into integer form for further operations, which is more challenging for beginners who need to calculate ET_a products urgently, and unfavorable for ET_a estimation at a large spatial and temporal scales.

To overcome the aforementioned disadvantages, this study developed a more user-friendly PySEBS, which has the following advantages compared with the conventional calculation method. The strengths are to (1) simplify the preprocessing process of remote sensing data and meteorological data, especially meteorological data can be directly interpolated from point-scale data to raster files; (2) develop a concise user interface that makes the input and output of data and modification of parameters more straightforward and convenient; and (3) reduce the time consumption greatly. Once the required parameters are set, the whole process will no longer require the users to manually input data year by year, and the ET_a results can be calculated automatically and continuously for many years on a regional scale. In addition, the newly developed PySEBS model can be used to calculate crop water productivity [30], which is very useful for land degradation assessment [53].

Although the PySEBS model performed relatively well in this study, there were some limitations: since the cover type primarily targeted in this study was spring maize, the calculations of ET_a in estimating other crops might be inadequate; another point is that the spatial and temporal resolutions of the remote sensing data used need to be further improved, and the spatial resolution of 500–1000 m is not sufficient to distinguish the evapotranspiration characteristics in areas with complex surface cover types, and the existence of mixed image elements may affect the estimation results to a certain extent. Finally, users can also use remote sensing data from other sources, such as Landsat and Sentinel satellites, rather than being limited to MODIS remote sensing data. However, some of the relevant equations in the Supplementary Materials, for example, Equation (3) for calculating surface albedo needs to be adjusted accordingly. Future research should pay more attention to the estimation of evapotranspiration on different surface cover types and the selection of remote sensing data with a higher resolution.

5. Conclusions

A scientific calculation software named PySEBS was developed to calculate ET_a on a regional scale. Its most important feature is that it can preprocess remote sensing data and meteorological data quickly, efficiently, and continuously, and calculate the regional ET_a on a daily basis. Detailed descriptions of the installation environment, input data requirements, selection method of meteorological data interpolation, formula sources and derivations, and operation procedures of the PySEBS software are presented in this study, which walk the users through the whole set-up and help them to understand the software principles. In addition, spring maize in Jilin Province was selected as the research object, and ET_a was calculated during the growing season of spring maize from 2001 to 2020. Finally, the spatio-temporal distribution patterns of ET_a during the growing season of spring maize in Jilin Province were mapped and analyzed in this study.

Results indicated that the multi-year average extraction accuracy of the spring maize planting area was 90.6% and that the overall R^2 between the statistical area of spring maize and the extracted area in all years was 0.81. The average cumulative ET_a of spring maize in the growing season in Jilin Province from 2001 to 2020 ranged from 475 to 544 mm, with a multi-year mean of 517 mm and a standard deviation mean of 43 mm. The highest ET_a was in July with a mean of 132 mm. On the spatial scale, the multi-year mean ET_a ranged from 391 to 693 mm, and the CV was mostly between 2% and 18%. The cities with the

largest multi-year average ET_a values were Tonghua, Jilin, and Liaoyuan, and all of them had ET_a over 530 mm. The multi-year average ET_a of spring maize growing season in Jilin Province in this study was 517 mm, which was similar to the results of other related studies in Jilin Province, and the values were within a reasonable range, indicating that the PySEBS software could estimate the ET_a values well. Therefore, PySEBS software can have useful applications in the spatio-temporal patterns of water consumption and irrigation demand in regional scales and associated water saving scenarios.

Supplementary Materials: The following supporting information can be downloaded at: <https://www.mdpi.com/article/10.3390/rs14215629/s1>, PySEBS V1.0.0 Actual Evapotranspiration (ET_a) Calculator User's Guide [7,18,31–42].

Author Contributions: Conceptualization, H.L. and Y.C.; methodology, H.L. and Y.C.; software, H.L. and P.R.; validation, H.L. and Y.C.; formal analysis, H.L. and Y.C.; investigation, H.L.; resources, F.H. and Y.C.; data curation, F.H.; writing—original draft preparation, H.L., Y.C. and Y.L.; writing—review and editing, H.L., Y.C., Y.L., G.W.M. and B.D.; visualization, H.L.; supervision, Y.C., B.L. and F.H.; project administration, B.L. and Y.C.; funding acquisition, Y.C. and F.H. All authors have read and agreed to the published version of the manuscript.

Funding: This research was funded by the Chinese Universities Scientific Fund under award numbers 1191-15051002, 1191-10092004, 1191-15052008, and 1191-31051204. The study was also supported by the National Key Research and Development Program of China under grant numbers 2016YFD0300801 and 2016YFD0300801013.

Institutional Review Board Statement: Not applicable.

Informed Consent Statement: Not applicable.

Data Availability Statement: PySEBS software and 2019 case data are freely distributed through a GitHub public repository (<https://github.com/haipengliuCAU/PySEBS>, accessed on 15 August 2022).

Acknowledgments: We thank the National Aeronautics and Space Administration (NASA) and the National Meteorological Information Center (NMIC) for providing the MODIS remote sensing data and meteorological data. We greatly appreciate four anonymous reviewers for their valuable comments and suggestions for improving this article.

Conflicts of Interest: The authors declare no conflict of interest.

References

1. Peng, L.Q.; Zeng, Z.Z.; Wei, Z.W.; Chen, A.P.; Wood, E.F.; Sheffield, J. Determinants of the ratio of actual to potential evapotranspiration. *Glob. Change Biol.* **2019**, *25*, 1326–1343. [[CrossRef](#)] [[PubMed](#)]
2. Tasumi, M. Estimating evapotranspiration using METRIC model and Landsat data for better understandings of regional hydrology in the western Urmia Lake Basin. *Agric. Water Manag.* **2019**, *226*, 105805. [[CrossRef](#)]
3. McMahan, T.A.; Peel, M.C.; Lowe, L.; Srikanthan, R.; McVicar, T.R. Estimating actual, potential, reference crop and pan evaporation using standard meteorological data: A pragmatic synthesis. *Hydrol. Earth Syst. Sci.* **2013**, *17*, 1331–1363. [[CrossRef](#)]
4. Xiang, K.Y.; Li, Y.; Horton, R.; Feng, H. Similarity and difference of potential evapotranspiration and reference crop evapotranspiration—A review. *Agric. Water Manag.* **2020**, *232*, 106043. [[CrossRef](#)]
5. Gutierrez-Ninahuan, C.; Gonzalez-Herrera, R. Software to analyze ET_o . Compilation of indirect methods. *Environ. Model. Softw.* **2021**, *142*, 105056. [[CrossRef](#)]
6. Dingman, S.L. *Physical Hydrology*, 1st ed.; Prentice Hall: Hoboken, NJ, USA, 1992.
7. Allen, R.G.; Pereira, L.S.; Raes, D.; Smith, M. *Crop Evapotranspiration—Guidelines for Computing Crop Water Requirements—FAO Irrigation and Drainage Paper 56*; FAO: Rome, Italy, 1998.
8. Bowen, I.S. The ratio of heat losses by conduction and by evaporation from any water surface. *Phys. Rev.* **1926**, *27*, 779–787. [[CrossRef](#)]
9. Thornthwaite, C.W.; Holzman, B. The determination of evaporation from land and water surfaces. *Mon. Weather Rev.* **1939**, *67*, 4–11. [[CrossRef](#)]
10. Penman, H.L. Natural evaporation from open water, bare soil and grass. *Proc. R. Soc. Lond. Ser. A* **1948**, *193*, 120–145. [[CrossRef](#)]
11. Monteith, J.L. Evaporation and environment. *Symp. Soc. Exp. Biol.* **1965**, *19*, 205–234.
12. Shuttleworth, W.J.; Wallace, J.S. Evaporation from sparse crops—an energy combination theory. *Q. J. R. Meteorol. Soc.* **1985**, *111*, 839–855. [[CrossRef](#)]

13. Dolman, A.J. A multiple-source land surface energy balance model for use in general circulation models. *Agric. For. Meteorol.* **1993**, *65*, 21–45. [[CrossRef](#)]
14. Choudhury, B.J.; Monteith, J.L. A four-layer model for the heat budget of homogeneous land surfaces. *Q. J. R. Meteorol. Soc.* **2010**, *114*, 373–398. [[CrossRef](#)]
15. Norman, J.M.; Kustas, W.P.; Humes, K.S. Source approach for estimating soil and vegetation energy fluxes in observations of directional radiometric surface temperature. *Agric. For. Meteorol.* **1995**, *77*, 263–293. [[CrossRef](#)]
16. Carlson, T. An overview of the "triangle method" for estimating surface evapotranspiration and soil moisture from satellite imagery. *Sensors* **2007**, *7*, 1612–1629. [[CrossRef](#)]
17. Bastiaanssen, W.G.M.; Menenti, M.; Feddes, R.A.; Holtslag, A.A.M. A remote sensing surface energy balance algorithm for land (SEBAL)—1. Formulation. *J. Hydrol.* **1998**, *212*, 198–212. [[CrossRef](#)]
18. Su, Z. The Surface Energy Balance System (SEBS) for estimation of turbulent heat fluxes. *Hydrol. Earth Syst. Sci.* **2002**, *6*, 85–99. [[CrossRef](#)]
19. Allen, R.G.; Tasumi, M.; Trezza, R. Satellite-based energy balance for mapping evapotranspiration with internalized calibration (METRIC)—Model. *J. Irrig. Drain. Eng. ASCE* **2007**, *133*, 380–394. [[CrossRef](#)]
20. Long, D.; Singh, V.P. A Two-source Trapezoid Model for Evapotranspiration (TTME) from satellite imagery. *Remote Sens. Environ.* **2012**, *121*, 370–388. [[CrossRef](#)]
21. Laipelt, L.; Kayser, R.H.B.; Fleischmann, A.S.; Ruhoff, A.; Bastiaanssen, W.; Erickson, T.A.; Melton, F. Long-term monitoring of evapotranspiration using the SEBAL algorithm and Google Earth Engine cloud computing. *ISPRS J. Photogramm. Remote Sens.* **2021**, *178*, 81–96. [[CrossRef](#)]
22. Du, J.; Song, K.S.; Wang, Z.M. Estimation of water consumption and productivity for rice through integrating remote sensing and census data in the Songnen Plain, China. *Paddy Water Environ.* **2015**, *13*, 91–99. [[CrossRef](#)]
23. Bhattarai, N.; Liu, T. LandMOD ET mapper: A new matlab-based graphical user interface (GUI) for automated implementation of SEBAL and METRIC models in thermal imagery. *Environ. Model. Softw.* **2019**, *118*, 76–82. [[CrossRef](#)]
24. Mhaweji, M.; Faour, G. Open-source Google Earth Engine 30-m evapotranspiration rates retrieval: The SEBALIGEE system. *Environ. Model. Softw.* **2020**, *133*, 104845. [[CrossRef](#)]
25. Ramirez-Cuesta, J.M.; Allen, R.G.; Intrigliolo, D.S.; Kilic, A.; Robison, C.W.; Trezza, R.; Santos, C.; Lorite, I.J. METRIC-GIS: An advanced energy balance model for computing crop evapotranspiration in a GIS environment. *Environ. Model. Softw.* **2020**, *131*, 104770. [[CrossRef](#)]
26. Ellsasser, F.; Roll, A.; Stiegler, C.; Hendrayanto; Hölscher, D. Introducing QWaterModel, a QGIS plugin for predicting evapotranspiration from land surface temperatures. *Environ. Model. Softw.* **2020**, *130*, 104739. [[CrossRef](#)]
27. Wu, F.; Wu, B.; Zhu, W.; Yan, N.; Ma, Z.; Wang, L.; Lu, Y.; Xu, J. ETWatch cloud: APIs for regional actual evapotranspiration data generation. *Environ. Model. Softw.* **2021**, *145*, 105174. [[CrossRef](#)]
28. Kayser, R.H.; Ruhoff, A.; Laipelt, L.; Kich, E.D.; Roberti, D.R.; Souza, V.D.; Rubert, G.C.D.; Collischonn, W.; Neale, C.M.U. Assessing geeSEBAL automated calibration and meteorological reanalysis uncertainties to estimate evapotranspiration in subtropical humid climates. *Agric. For. Meteorol.* **2022**, *314*, 108775. [[CrossRef](#)]
29. Huang, C.L.; Li, Y.; Gu, J.; Lu, L.; Li, X. Improving estimation of evapotranspiration under water-limited conditions based on SEBS and MODIS data in arid regions. *Remote Sens.* **2015**, *7*, 16795–16814. [[CrossRef](#)]
30. Ren, P.P.; Huang, F.; Li, B.G. Spatiotemporal patterns of water consumption and irrigation requirements of wheat-maize in the Huang-Huai-Hai Plain, China and options of their reduction. *Agric. Water Manag.* **2022**, *263*, 107468. [[CrossRef](#)]
31. Han, X.P.; Wang, Y.Q.; Bao, L. Introduction of ILWIS functions and its scanning digital application. *Lab. Sci.* **2008**, *2*, 107–109. [[CrossRef](#)]
32. Liang, S.L. Narrowband to broadband conversions of land surface albedo I Algorithms. *Remote Sens. Environ.* **2001**, *76*, 213–238. [[CrossRef](#)]
33. Yang, X.T. Evapotranspiration Estimating using Remote Sensing and Spatial-Temporal Distribution of Evapotranspiration in Golmud River Basin Based on SEBS Model. Master's Thesis, Chang'an University, Xi'an, China, 2017.
34. Wu, Y.L. Research on Retrieving and Spatial-Temporal Changes of Evaporation Estimation in the Yellow River Delta Based on Refined SEBS Model. Master's Thesis, China University of Petroleum, Beijing, China, 2010.
35. Li, X. Estimation of Sensible Heat Flux Based on SEBS Model and Its Application for Drought Monitoring. Master's Thesis, Nanjing University of Information Engineering, Nanjing, China, 2012.
36. Hao, J.W. Study on Evapotranspiration Based on SEBS Model in Handan. Master's Thesis, Hebei University of Engineering, Handan, China, 2018.
37. Jobson; Harvey, E. Evaporation into the atmosphere: Theory, history, and applications. *Eos Trans. Am. Geophys. Union* **1982**, *63*, 1223. [[CrossRef](#)]
38. Hogstrom, U. Non-dimensional wind and temperature profiles in the atmospheric surface layer: A re-evaluation. *Bound. Layer Meteor.* **1988**, *42*, 55–78. [[CrossRef](#)]
39. Kader, B.A.; Yaglom, A.M. Mean fields and fluctuation moments in unstably stratified turbulent boundary layers. *J. Fluid Mech.* **1990**, *212*, 637–662. [[CrossRef](#)]
40. Beljaars, A.C.M.; Holtslag, A.A.M. Flux parameterization over land surfaces for atmospheric models. *J. Appl. Meteorol.* **1991**, *30*, 327–341. [[CrossRef](#)]

41. VandenHurk, B.; Holtslag, A.A.M. On the bulk parameterization of surface fluxes for various conditions and parameter ranges. *Bound. Layer Meteor.* **1997**, *82*, 119–134. [[CrossRef](#)]
42. Brutsaert, W. Aspects of bulk atmospheric boundary layer similarity under free-convective conditions. *Rev. Geophys.* **1999**, *37*, 439–451. [[CrossRef](#)]
43. Shuttleworth, W.J. FIFE: The variation in energy partition at surface flux sites. *IAHS* **1989**, *186*, 67–74.
44. Sugita, M.; Brutsaert, W. Daily evaporation over a region from lower boundary layer profiles measured with radiosondes. *Water Resour. Res.* **1991**, *27*, 747–752. [[CrossRef](#)]
45. Crago, R.D. Comparison of the evaporative fraction and the Priestley-Taylor alpha for parameterizing daytime evaporation. *Water Resour. Res.* **1996**, *32*, 1403–1409. [[CrossRef](#)]
46. Li, G. Estimation Evapotranspiration in Yingtan Agricultural Watershed using SEBAL and SEBS Model. Master's Thesis, Nanjing University of Information Engineering, Nanjing, China, 2014.
47. Guo, C.M.; Ren, J.Q.; Zhang, T.L.; Yu, H. Dynamic change of evapotranspiration and influenced factors in the spring maize field in Northeast China. *Chin. J. Agrometeorol.* **2016**, *37*, 400–407. [[CrossRef](#)]
48. Qiu, M.J.; Guo, C.M.; Wang, D.N.; Yuan, F.X.; Qu, S.M.; Ren, J.Q.; Li, Z.H.; Mu, J. Variation of effective precipitation and water deficit index in maize growing season in Jilin Province during 1960–2015. *Agric. Res. Arid. Reg.* **2018**, *36*, 237–280. [[CrossRef](#)]
49. Zhang, Y.; Wang, L.X.; Li, Q.; Hu, Z.H.; Guo, C.M.; Ren, J.Q. Irrigation simulation of spring maize in central and western of Jilin Province based on WOFOST model. *Chin. J. Agrometeorol.* **2018**, *39*, 411–420. [[CrossRef](#)]
50. Liu, Y. Simulation and Applications of Maize Evapotranspiration Based on SIMETAW Model. Master's Thesis, Chinese Academy of Agricultural Sciences, Beijing, China, 2011.
51. Jiang, H.; Liu, S.R.; Sun, P.S.; An, S.Q.; Zhou, G.Y.; Li, C.Y.; Wang, J.X.; Yu, H.; Tian, X.J. The influence of vegetation type on the hydrological process at the landscape scale. *Can. J. Remote Sens.* **2004**, *30*, 743–763. [[CrossRef](#)]
52. Seguin, B.; Becker, F.; Phulpin, T.; Gu, X.F.; Guyot, G.; Kerr, Y.; King, C.; Lagouarde, J.P.; Otle, C.; Stoll, M.P. IRSUTE: A minisatellite project for land surface heat flux estimation from field to regional scale. *Remote Sens. Environ.* **1999**, *68*, 357–369. [[CrossRef](#)]
53. Schillaci, C.; Jones, A.; Vieira, D.; Munafò, M.; Montanarella, L. Evaluation of the United Nations sustainable development goal 15.3.1 indicator of land degradation in the European Union. *Land Degrad. Dev.* **2022**, 1–19. [[CrossRef](#)]